

c-axis magnetotransport in CeCoIn₅

A. Malinowski,^{1,2} M. F. Hundley,¹ C. Capan,^{1,*} F. Ronning,¹ R. Movshovich,¹ N. O. Moreno,¹ J. L. Sarrao,¹ and J. D. Thompson¹

¹*Materials Science and Technology Division, Los Alamos National Laboratory, Los Alamos, New Mexico 87545, USA*

²*Institute of Physics, Polish Academy of Sciences, 02 668 Warsaw, Poland*

(Dated: May 16, 2018)

We present the results of out-of-plane electrical transport measurements on the heavy fermion superconductor CeCoIn₅ at temperatures from 40 mK to 400 K and in magnetic field up to 9 T. For $T < 10$ K transport measurements show that the zero-field resistivity ρ_c changes linearly with temperature and extrapolates nearly to zero at 0 K, indicative of non-Fermi-liquid (nFL) behavior associated with a quantum critical point (QCP). The longitudinal magnetoresistance (LMR) of CeCoIn₅ for fields applied parallel to the c-axis is negative and scales as $B/(T + T^*)$ between 50 and 100 K, revealing the presence of a single-impurity Kondo energy scale $T^* \sim 2$ K. Beginning at 16 K a small positive LMR feature is evident for fields less than 3 tesla that grows in magnitude with decreasing temperature. For higher fields the LMR is negative and increases in magnitude with decreasing temperature. This sizable negative magnetoresistance scales as B^2/T from 2.6 K to roughly 8 K, and it arises from an extrapolated residual resistivity that becomes negative and grows quadratically with field in the nFL temperature regime. Applying a magnetic field along the c-axis with $B > B_{c2}$ restores Fermi-liquid behavior in $\rho_c(T)$ at T less than 130 mK. Analysis of the T^2 resistivity coefficient's field-dependence suggests that the QCP in CeCoIn₅ is located *below* the upper critical field, inside the superconducting phase. These data indicate that while high- T c-axis transport of CeCoIn₅ exhibits features typical for a heavy fermion system, low- T transport is governed both by spin fluctuations associated with the QCP and Kondo interactions that are influenced by the underlying complex electronic structure intrinsic to the anisotropic CeCoIn₅ crystal structure.

PACS numbers: 71.27.+a, 73.43.Qt, 75.40.-s, 74.70.Tx

I. INTRODUCTION

Extensive evidence for departures from the temperature-dependencies characteristic of Fermi-liquid (FL) behavior in the thermodynamic properties of d - and f -metals has been collected over the last fifteen years.¹ A key observation is that both the Sommerfeld coefficient, $\gamma = C/T$, and the Pauli susceptibility χ increase with decreasing temperature and show no sign of entering a T -independent FL regime down to the lowest achievable temperatures. Another primary indication of non-Fermi-liquid (nFL) behavior in heavy fermion (HF) systems is provided by the low-temperature non-quadratic (in some systems close to linear) temperature dependence exhibited by the resistivity in these compounds.² This transport behavior may link the heavy-fermion compounds with the copper oxide superconductors where a T -linear resistivity is observed over a wide temperature range that often extrapolates to zero at $T = 0$.^{3,4}

Theories trying to explain nFL behavior can be divided into three categories:¹ (1) models that describe the behavior expected near a quantum critical point (QCP), (2) multichannel single-impurity Kondo models, and (3) models based on disorder. These general categories are not exclusive; an anisotropic multichannel single-impurity model also yields a QCP,⁵ while disorder plays an important role in models based on a single-impurity mechanism,^{6,7} in models incorporating interactions between magnetic ions,⁸ and in theories describing

spin fluctuations near a QCP.⁹ The scenario attracting the most attention at present associates nFL behavior with a nearby magnetic quantum critical point.¹⁰ A QCP can often be achieved by doping a pure system chemically, as in the archetype HF compound UPt₃ doped with Pd (Ref. 11), La-doped CeRu₂Si₂ (Ref. 12), Au-doped CeCu₆, (Ref. 13) or Si-doped CeCoGe₃ (Ref. 14). This introduces additional disorder and makes the situation even more challenging for theory because of the need to build a unified picture from the aforementioned competing mechanisms. Using magnetic field – where possible – as a tuning parameter avoids at least some of the complications associated with doping. Using the field-tuning approach has the added advantage of being continuously tunable. While a QCP, by definition, produces a $T = 0$ phase transition, the finite-temperature properties of the system are also strongly affected.¹⁵ These properties can be examined with a scaling analysis¹⁶ in order to investigate the nature of the QCP.

CeCoIn₅ is one such system where a QCP can be induced by magnetic field. Heat capacity¹⁷ and de Haas-van Alphen^{18,19} measurements reveal that CeCoIn₅ is a heavy-electron system. This compound is an ambient-pressure superconductor with the highest T_c (2.3 K) among the Ce-based HF materials known to-date.¹⁷ The unusual magnetic and thermodynamic properties, both in the normal and superconducting state, are attracting great interest in this compound. The specific heat C ,^{17,20} thermal conductivity κ ,²⁰ and spin-lattice relaxation time T_1 (Ref. 21) all display power-law tempera-

ture dependencies below T_c , while angle-dependent thermal conductivity²² and specific-heat data²³ show four-fold modulation. These results indicate that CeCoIn₅ is quite likely an unconventional line-node superconductor. In the normal state C/T varies with temperature as $-\ln T$ (Ref. 17,24,25), $1/T_1T$ is proportional to $T^{-3/4}$ (Ref. 21,26), χ varies as $T^{-0.42}$ for $B \parallel c$,²⁷ and the ab-plane resistivity varies linearly with temperature.^{24,28} These nFL properties have been attributed to the presence of a QCP in the magnetic phase diagram. No long-range AFM order has been detected in CeCoIn₅, although AFM correlations have been observed²¹, and these correlations may play a crucial role in producing the nFL behavior.²⁹ Magnetic-field and temperature-dependent specific-heat²⁵ and ab-plane transport³⁰ measurements suggest that the magnetic QCP is located close to the upper superconducting critical field, B_{c2} . The origin of the QCP and the nature of the quantum fluctuations in CeCoIn₅ are not yet established.

Although CeCoIn₅ provides a unique opportunity to study nFL behavior without complications caused by alloying, a careful separation of co-existing effects is still necessary when analyzing measured properties. For instance, a systematic study at zero-field has revealed competing energy scales between single-ion Kondo and inter-site coupling effects.²⁴ On the other hand, our recent in-plane transport study³¹ has shown that the Hall effect in the Ce-115 materials is strongly influenced by the conventional electronic-structure that these materials share with their non-magnetic La-analogs. This suggests that when analyzing CeCoIn₅ MR data it is important to account for conventional MR effects (as determined from LaCoIn₅ MR data) before associating any unusual effects with Kondo or QCP physics.

In this paper we present the results of CeCoIn₅ c-axis magnetoresistance measurements carried out with the aim of clarifying the origin of nFL behavior. The measurements were made in field strengths up to 9 T and at temperatures from 400 K down to 40 mK. In zero field the resistivity along the c-axis, ρ_c , varies linearly with T from 40 mK to 8 K and extrapolates essentially to zero at 0 K. The linear temperature dependence of both ρ_{ab} and ρ_c is consistent with an interplay of strongly anisotropic scattering due to anisotropic 3D spin fluctuations and isotropic impurity scattering. Applying a magnetic field along the c-axis produces a T^2 resistivity, indicating that FL behavior has been restored. Careful analysis of the T^2 -coefficient field dependence suggests that the QCP is located below the upper c-axis critical field, *within* the superconducting phase. The MR field-dependence below 8 K shows subtle but important deviations from canonical heavy-fermion behavior that may be associated with magnetic QCP fluctuations. In this temperature range the longitudinal magnetoresistance (LMR) scales with B and T as B^2/T due, mainly, to a negative extrapolated residual resistivity that increases quadratically with field; at higher temperatures this scaling breaks down, possibly due to a variation in quenching of Kondo scattering

by field for different charge-carrier bands. For T greater than the coherence temperature (~ 45 K) the LMR again shows single-impurity Kondo behavior; the MR data indicate that the single-ion Kondo scale T^* is roughly 2 K.

II. EXPERIMENT

Single crystals of CeCoIn₅ and LaCoIn₅ were grown from an excess In flux, as described in Ref. [17]. Excess indium was eliminated by etching the samples in 3:1 HCl:H₂O solution. CeCoIn₅ specimens were polished into rectangular shape, while LaCoIn₅ samples were left in their as-grown plate-like shape. All specimens were pre-screened to ensure that there was no sign of an In superconducting transition at 3.2 K. Electrical contacts in a standard linear four-probe configuration were prepared with silver epoxy while silver paste was used when employing a van der Pauw configuration.

Two CeCoIn₅ specimens were used in performing anisotropic $\rho_{xx}(B, T)$ and $\rho_{xy}(B, T)$ (Hall resistivity) measurements, hereafter denoted as samples I and II. The in-plane and out-of-plane resistivities of CeCoIn₅ were determined on crystallographically oriented sample I via the anisotropic van der Pauw method.^{32,33} Sample I had a thickness of 0.2 mm and lengths of 0.5 and 0.8 mm along the c-axis and a-axis, respectively. The measurements in magnetic field were carried out on sample II (0.1×0.2×0.6 mm³), with the longest dimension along the c-axis. LaCoIn₅ samples had thickness varying from 0.03 to 0.06 mm (along the c-axis) and dimensions of 0.5×1 mm² in the ab-plane. The ρ_{ab} vs. T curves for LaCoIn₅ were normalized to the average value of the room-temperature resistivity as determined from anisotropic van der Pauw measurements.

The temperature and field variation of resistivity from 1.8 K to 400 K and in fields up to 9 T were studied using a Quantum Design PPMS cryostat while measurements from 40 mK to 2 K were carried out in a ³He/⁴He dilution refrigerator. In both cases resistance measurements were made with an LR-700 ac resistance bridge. The magnetic field was applied parallel to the current flowing through the sample. The advantage of using this longitudinal configuration is that it minimizes or eliminates the influence of “classical” magnetoresistance effects arising from the Lorentz force. Magnitudes of the magnetoresistance reported here are defined in the usual way as $\Delta\rho/\rho_0 = [\rho(B) - \rho(B=0)]/\rho(B=0)$.

III. RESULTS

The out-of-plane (ρ_c) and in-plane (ρ_{ab}) resistivities of CeCoIn₅, measured simultaneously on a single crystal via the anisotropic van der Pauw technique,³³ together with the in-plane resistivity of the non-magnetic analog, LaCoIn₅, are depicted in Fig. 1 (a). The in-plane resis-

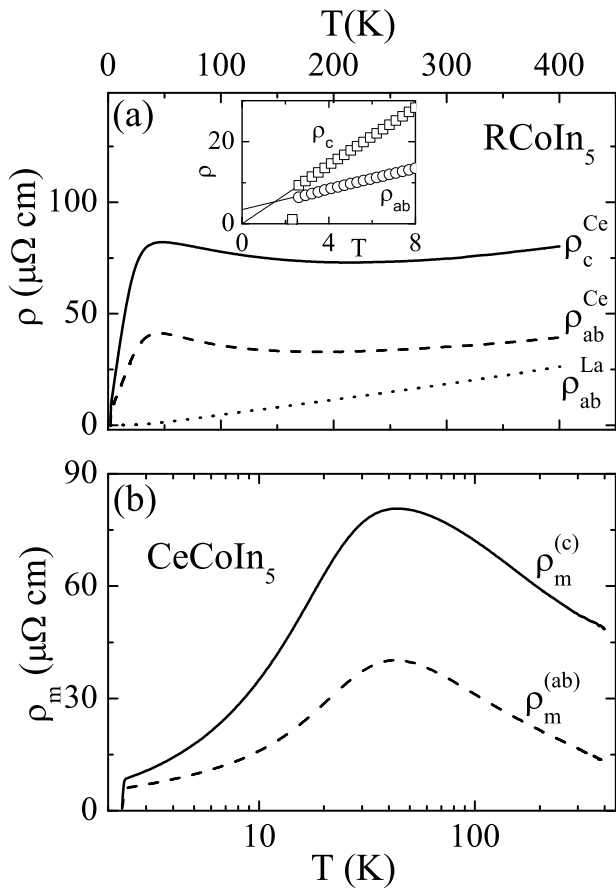


FIG. 1: (a) Resistivity of CeCoIn₅ (ρ_{ab} and ρ_c) and LaCoIn₅ (ρ_{ab}) plotted as a function of temperature. The inset shows the out-of-plane and in-plane resistivities of CeCoIn₅ for $T \leq 8$ K along with linear extrapolations down to zero temperature. (b) The ab-plane ($\rho_m^{(ab)}$) and c-axis ($\rho_m^{(c)}$) magnetic resistivities of CeCoIn₅ plotted as a function of temperature.

tivity of LaCoIn₅ decreases almost linearly with decreasing temperature and saturates below 10 K to a sample-dependent value of roughly $0.05 \mu\Omega$ cm. The residual resistivity ratio (~ 350) indicates that the crystals grown via the flux-growth technique are of high-quality. We were unable to measure ρ_c for LaCoIn₅ because the crystals grow as extremely thin plates. An estimate of the LaCoIn₅ c-axis resistivity can be determined from LaRhIn₅ transport data. For LaRhIn₅ it was found previously that the anisotropy ratio $\rho_c/\rho_{ab} \sim 1.2$ is nearly T -independent, suggesting that the inherent nonmagnetic electronic anisotropy is relatively small for the RMI₅ (R=Ce,La; M=Co,Ir,Rh) structure.³⁴ In the following we assume that ρ_c can be quite reasonably approximate as $1.2\rho_{ab}$ for LaCoIn₅ as well.

The temperature-dependence of the CeCoIn₅ zero-field resistivity is much more complex than that of its nonmagnetic analog. At room temperature ρ_c is 2.1 times larger than ρ_{ab} , indicating that magnetic scattering in CeCoIn₅ is modestly anisotropic. Between 400 K and 45 K ρ_c and ρ_{ab} are weakly T -dependent, exhibiting a

very gradual minimum centered at roughly 200 K. Below ~ 45 K the resistivity in both directions start to decrease rapidly with decreasing T . This behavior is typical for Kondo lattice systems and indicates the development of Kondo coherence effects.³⁵ Below ~ 10 K ρ_c and ρ_{ab} vary linearly with temperature. Although ρ_{ab} extrapolates to a finite value at zero temperature ($3.8 \mu\Omega$ cm for the sample I, presented in Fig. 1), the out-of-plane resistivity of CeCoIn₅ extrapolates nearly to zero (see the inset to Fig. 1 (a)).

If we assume that Matthiessen's rule is valid, the magnetic parts of CeCoIn₅'s zero-field resistivities in both crystallographic directions, $\rho_m^{(c)}$ and $\rho_m^{(ab)}$, can be obtained by subtracting ρ_{La} from ρ_{Ce} . The in-plane and c-axis magnetic resistivities of CeCoIn₅ calculated in this manner are shown in Fig. 1 (b). At high temperatures both $\rho_m^{(c)}$ and $\rho_m^{(ab)}$ vary as $-\ln(T)$, consistent with single-impurity Kondo scattering.³⁶ Throughout the whole temperature range displayed in the figure $\rho_m^{(c)}$ is higher than $\rho_m^{(ab)}$, and the magnetic anisotropy ratio $r_m \equiv \rho_m^{(c)}/\rho_m^{(ab)}$ drops with decreasing temperature. The anisotropy ratio is ~ 3.2 at 295 K, decreases with decreasing T , and reaches a local minimum ($r_m = 2$) at the temperature where the resistance shows a coherence maximum (42 K). At still lower temperatures r_m drops gradually, reaching a value of $r_m = 1.4$ at 2.5 K. Apart from the T -dependent anisotropy ρ_m is qualitatively the same in both directions, with the coherence peak at 42 K.

The differences between the resistivities of LaCoIn₅ and CeCoIn₅ are even more evident when measurements are made in a magnetic field. The T -dependent magnetoresistance of LaCoIn₅ varies with temperature in a manner typical for a conventional metal. In the whole T range studied, 2 K – 300 K, the ab-plane LMR is positive. Its magnitude at 9 T increases smoothly with decreasing T , changing from a room-temperature value of $\Delta\rho/\rho_0 = +0.24\%$ to a 10 K value of $\Delta\rho/\rho_0 = +33\%$. Below 10 K the LMR decreases slightly in magnitude, attaining a 9 T value of $+29\%$ at 2 K. The transverse magnetoresistance (TMR) in the ab-plane ($B \parallel c$) shows the same temperature behavior as the LMR and is roughly ten times bigger at all temperatures. A more detailed look at the LaCoIn₅ MR temperature and field dependence will be presented in section IV A.

The field-dependent longitudinal magnetoresistance of CeCoIn₅ measured at various temperatures with $B \parallel c$ is shown in Fig. 2; the data differ markedly from that of LaCoIn₅. The LMR is positive at 350 K, varies quadratically with field, and has a 9 T value of $+0.12\%$. The LMR decreases with decreasing temperature, and it becomes negative at 110 K. It stays negative in the high field region ($B > 3$ T) down to the lowest temperature in the normal state, with a magnitude that grows with decreasing T ; just above T_c the MR achieves a 9 T value of -21% . A positive feature is also evident in the LMR data below 16 K for $H < 3$ T, as highlighted in the inset to Fig. 2. Although small compared to the high-field

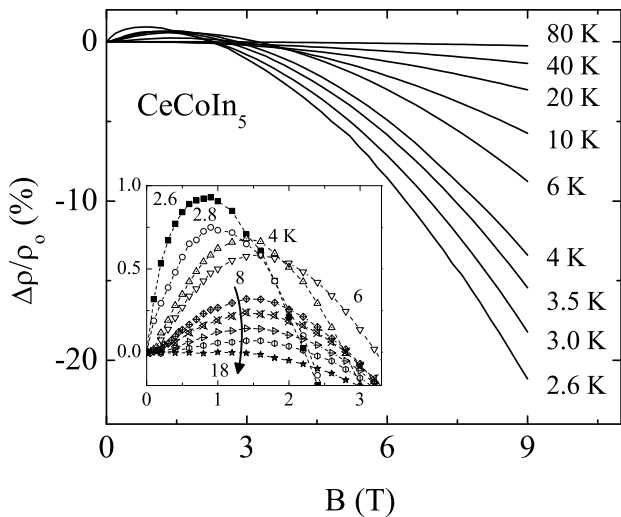


FIG. 2: Longitudinal magnetoresistance of CeCoIn₅ plotted as a function of applied field. The low-field region is magnified in the inset.

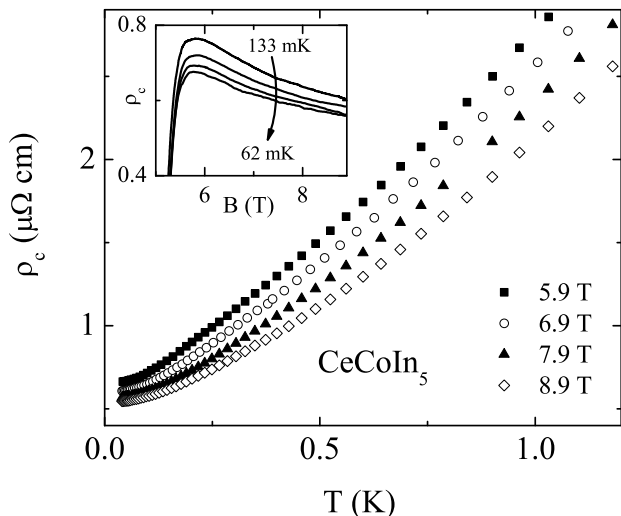


FIG. 3: Low-temperature *c*-axis resistivity of CeCoIn₅ measured at various magnetic fields as a function of temperature. The field was applied parallel to the current direction. The inset shows the *c*-axis resistivity plotted vs. field at (from top to bottom): 133, 106, 82 and 62 mK.

negative magnetoresistance, the positive feature grows in size with decreasing temperature, reaching a maximum of 1% just above T_c .

The most dramatic change in the resistivity of CeCoIn₅ is revealed when superconductivity is suppressed by applying a magnetic field. In zero field ρ_c varies linearly with temperature from 8 K down to T_c , indicative of nFL behavior. Extending the normal state down to lower T by applying a magnetic field along the *c*-axis alters this temperature dependence in an important way. This is

shown in Fig. 3 where $\rho_c(T)$ is plotted for fields greater than $B_{c2} = 5$ T. The curvature in $\rho_c(T)$ visible in the low- T region in Fig. 3 clearly indicates a departure from a linear T -dependence to one of the form $\rho_c \sim T^n$, with $n > 1$. At 5.9 T, $\rho_c(T)$ is proportional to T^2 below ~ 130 mK, indicating that a field-induced FL state has been achieved. The FL regime extends to 0.2 K in a 8.9 T field (see Fig. 9). The LMR in this temperature region is negative in the normal state, as shown in the inset to Fig. 3. This differs from the positive MR seen in low- T ab-plane transport measurements.³⁰

IV. DISCUSSION

In analyzing the MR data of CeCoIn₅ it is very important to separate field effects associated with many-body or magnetic interactions from conventional effects intrinsic to the complex RCoIn₅ electronic structure. As such, we will start by analyzing the LaCoIn₅ magnetoresistance in section IV A. By separating the MR of CeCoIn₅ into conventional and magnetic components we can reveal the presence of a single-impurity Kondo scale T^* in the data; this is discussed in section IV B. The zero field resistivity at low temperatures along the *c*-axis is analyzed in section IV C and compared with $\rho_{ab}(T)$. The magnetoresistance in the coherence regime is a subject of section IV D. Lastly, section IV E is devoted to the restoration of FL behavior by applying a magnetic field.

A. The magnetoresistance of LaCoIn₅

Above 20 K the magnetoresistance intrinsic to the RCoIn₅ electronic structure, given by the MR of LaCoIn₅, is a significant part of the total CeCoIn₅ MR. At 50 K, for example, the MR of LaCoIn₅ accounts for roughly 20% of the total MR exhibited by CeCoIn₅ in 9 T. Thus, before analyzing CeCoIn₅'s MR, we focus in this section on the magnetoresistance of its nonmagnetic analog.

The transverse and longitudinal ab-plane MR of LaCoIn₅ measured at temperatures from 300 K down to 20 K and in fields to 9 tesla are plotted as a function of B divided by the zero-field resistivity (ρ_0) in Fig. 4. The data clearly collapse onto a common curve, indicating that Kohler's rule,³⁷

$$\frac{\Delta\rho}{\rho_0} = F\left(\frac{B}{\rho_0}\right), \quad (1)$$

(where $F(x)$ is an unspecified function that depends on details of electronic structure) is fulfilled in LaCoIn₅ over a wide range of T encompassing an almost two order-of-magnitude variation in ρ_0 . Changes in temperature evidently alter the magnitude of the relaxation time, τ , by the same factor for all electron wave vectors, \vec{k} , without altering the form of $\tau(\vec{k})$.³⁸ The literature on magnetoresistance in metals focuses far more attention on applying

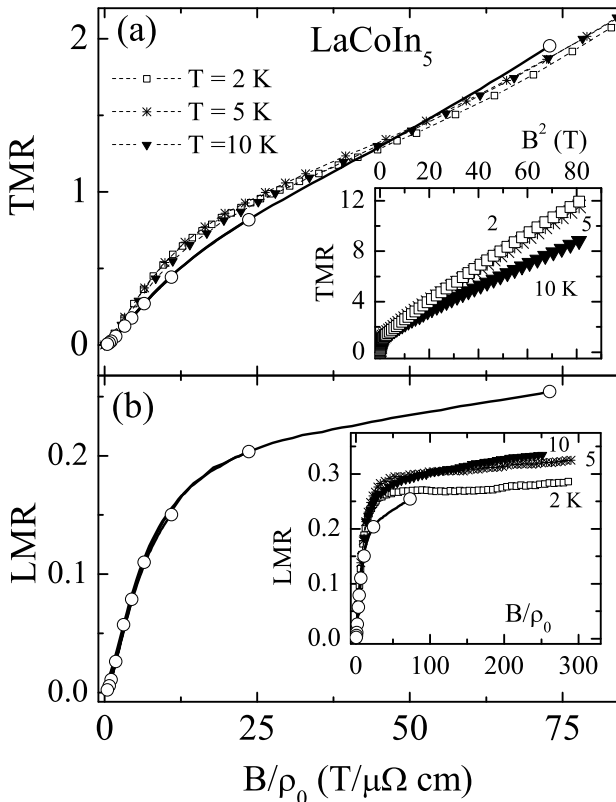


FIG. 4: (a) Transverse ($\vec{B} \parallel c$) and (b) longitudinal ($\vec{B} \parallel$ ab-plane and current) ab-plane magnetoresistance of LaCoIn_5 as a function of $B/\rho(B=0)$. The open circles in both panels show the 9 T magnetoresistance for (from left to right) $T = 300, 200, 150, 100, 70, 60, 50, 40, 30$ and 20 K, respectively. The solid line in both panels correspond to field-swept (0 to 9 T) MR data taken at the temperatures listed above; these field-sweeps are indistinguishable from one another, indicating that the MR of LaCoIn_5 obeys Kohler’s rule. MR data at 2, 5, and 10 K are also shown in (a) and the inset to (b) as a function of $B/\rho(B=0)$. The inset to (a) shows the transverse MR at 2, 5, and 10 K as a function of B^2 .

Kohler’s rule to the transverse configuration, and all but ignores the longitudinal configuration. It is worth noting, however, that the scaling argument describing the way in which the trajectory of the charge carriers is altered when the field B and the scattering rate $1/\tau$ are simultaneously increased by the same factor can be applied to *any* measured resistivity. As such, Eq. 1 can, in principle, be applied to *any* component of the resistivity tensor.³⁹ Deviations from Kohler’s rule are evident in the LaCoIn_5 MR data below 20 K. This is the same T region where the $\rho(T)$ curve becomes saturated, i.e. where residual impurity scattering begins to dominate electron-phonon scattering. A change in the dominant scattering mechanism leads, presumably, to an alteration in $\tau(\vec{k})$ below 20 K, resulting in modest deviations from Kohler’s rule.³⁸

As shown in the insets to Fig. 4 the low temperatures/high-field ab-plane MR of LaCoIn_5 becomes strongly anisotropic, and the behavior in the high-

field limit reflects the underlying Fermi surface topology intrinsic to the “115” structure. The LMR ($H \perp c$) at 2, 5 and 10 K saturates in high fields while the TMR ($H \parallel c$) increases approximately as B^2 without any sign of saturation when measured in fields up to 9 tesla. In a compensated metal (such as LaCoIn_5) where the area of hole and electron Fermi surfaces are equal, the TMR is expected to vary quadratically with B in the high-field limit when all orbits in planes normal to the applied field direction are closed.⁴⁰ The electron and hole Fermi surfaces in La-115 and Ce-115 materials are very complex,^{19,41,42} and both de Haas-van Alphen (dHvA) measurements and band-structure calculations indicate that the complex FS topology of LaRhIn_5 is dominated by corrugated electron-like cylindrical orbits that run along the c -axis.⁴¹ In such a situation the orbits in the ab-plane ($\vec{B} \parallel c$ -axis) are indeed closed, offering a simple explanation⁴³ for both the B^2 -dependence of the ab-plane TMR and the linear B -dependence of the Hall voltage reported recently.³¹ For a magnetic field applied perpendicular to the axis of a corrugated cylinder, the LMR is expected to saturate in the high-field limit.⁴⁴ This tendency is observed in the LaCoIn_5 MR when a field is applied in the ab-plane (see the inset to Fig. 4(b)). Hence, the directional dependence of the low- T MR in LaCoIn_5 is consistent with the cylindrical Fermi surface topology observed in dHvA measurements.

B. Single impurity regime of CeCoIn_5 .

By utilizing our knowledge of the MR of LaCoIn_5 it is possible to examine the CeCoIn_5 magnetoresistance components that stem from Kondo or other magnetic interactions. Again, assuming that Matthiessen’s rule is valid at finite field, we can simplify the MR problem by decomposing the total B -dependent resistivity of CeCoIn_5 , $\rho_{\text{tot}}(B)$, into two independent parts: $\rho_{\text{tot}}(B) = \rho_{\text{mag}}(B) + \rho_{\text{La}}(B)$; $\rho_{\text{mag}}(B)$ here is the magnetic-scattering contribution to the overall resistivity. We assume that the contribution of all other mechanisms can be approximated by the field-dependent resistivity of LaCoIn_5 , $\rho_{\text{La}}(B)$. The similarity between the electronic structures of CeRhIn_5 and LaRhIn_5 as observed in dHvA measurements^{19,41} corroborates this supposition. Next we define the magnetic part of the magnetoresistance, MR_{mag} , as

$$\text{MR}_{\text{mag}} = \frac{\Delta\rho_{\text{mag}}(B)}{\rho_{\text{mag}}(0)} = \frac{\rho_{\text{mag}}(B) - \rho_{\text{mag}}(0)}{\rho_{\text{mag}}(0)}. \quad (2)$$

In determining the magnetic longitudinal magnetoresistance of CeCoIn_5 (LMR_{mag}) we are forced to infer the c -axis B and T -dependent resistivity of LaCoIn_5 from ab-plane data because the La-analog sample thickness precludes making c -axis transport measurements. As discussed in the previous section, Fermi surface anisotropy only influences the magnetoresistance of LaCoIn_5 in the

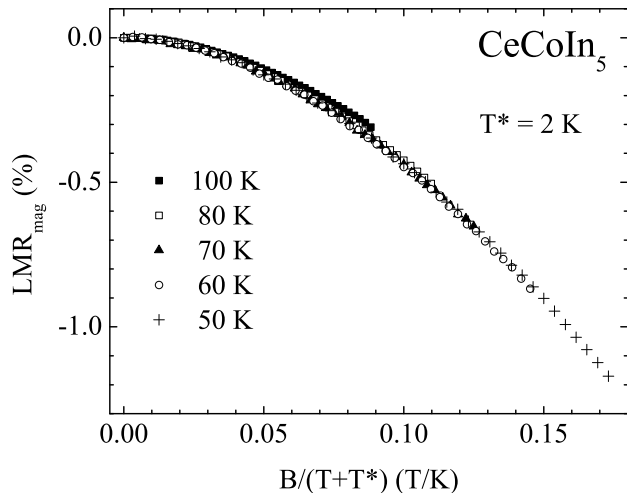


FIG. 5: f -electron contribution to the CeCoIn_5 longitudinal MR as a function of $B/(T+T^*)$, with $T^* = 2$ K.

low- T region. As such it is reasonable to assume that the c -axis and ab -plane magnetoresistance of LaCoIn_5 will be similar above ~ 20 K.

By following this recipe we find that the magnetic contribution to the longitudinal MR of CeCoIn_5 is negative below 200 K, varies quadratically with field, and grows in magnitude with decreasing temperature; for example, in a field of 9 tesla, the magnetic contribution to the longitudinal MR is -0.3% and -1.2% at 100 and 50 K, respectively. A negative MR that grows with decreasing temperature and increasing field is consistent with single-ion Kondo behavior.⁴⁵ Thus it is natural to carry out a scaling analysis of the LMR_{mag} data as suggested by the Bethe-ansatz solution of the Coqblin-Schrieffer model.^{45,46} In this single-impurity Kondo model the relative magnetoresistance depends on B and T only through the ratio $B/(T+T^*)$,

$$\frac{\Delta\rho(B,T)}{\rho(0,T)} = f\left(\frac{B}{T+T^*}\right), \quad (3)$$

where T^* plays the role of the single-ion Kondo temperature. In Fig. 5 we show that all $\text{LMR}_{mag}(B)$ curves between 50 K and 100 K can be superimposed onto a single unique curve when the data are scaled according to Eq. (3). Scaling works best for $T^* = (2 \pm 2)$ K. Although this value is a relatively small number when compared with the temperature range of interest, the quality of the scaling overlap begins to deteriorate when T^* is changed to values greater than 4 K. The temperature-range over which the MR data scale coincides roughly with the region of $-\log T$ behavior exhibited by ρ_m (see Fig. 1). The presence of a small single-impurity Kondo energy scale of roughly 1 to 2 K was reported in a systematic study of the zero-field resistivity, magnetic susceptibility, and specific heat of $\text{Ce}_{1-x}\text{La}_x\text{CoIn}_5$ (Ref. 24). The Kondo energy-scale was found to be essentially constant from the dilute limit ($x \rightarrow 1$) to the Kondo lattice

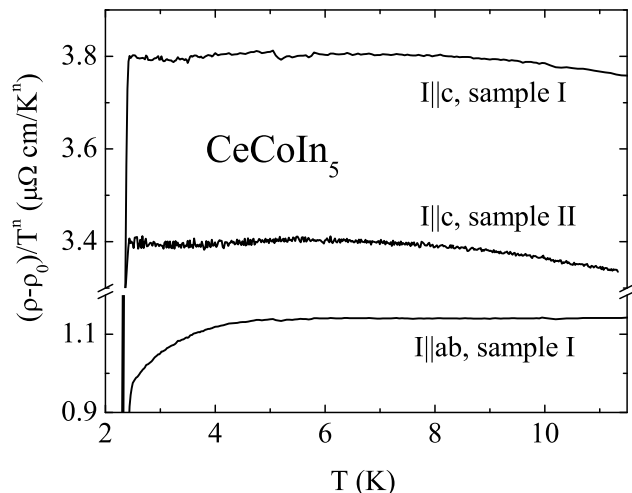


FIG. 6: Zero field resistivity of CeCoIn_5 plotted as $(\rho - \rho_0)/T^n$ vs. T . The upper and lower curves show ρ_{ab} and ρ_c of sample I as measured via the anisotropic van der Pauw method, while the middle curve depicts ρ_c for sample II. The best fit for the ab -plane data (corresponding to a horizontal line) occurs for $\rho_0 = 3.8 \mu\Omega \text{ cm}$, while fits to the c -axis data lead to slightly negative ρ_0 values: $\rho_0 = -0.30$, and $-0.39 \mu\Omega \text{ cm}$ for sample I, and II, respectively

limit ($x \rightarrow 0$). Hence, by properly accounting for conventional non-magnetic contributions to the MR, we are able to discern the single-impurity energy scale in the overall magnetotransport properties of CeCoIn_5 .

C. Transport at zero field in non-Fermi-liquid regime

In this section we examine the influence of AFM-fluctuations, dimensionality, and disorder in the low temperatures zero-field transport of CeCoIn_5 where in-plane^{25,30} and out-of-plane resistivity data clearly show evidence of nFL behavior. We fit the low- T data to the form

$$\rho(T) = \rho_0 + AT^n \quad (4)$$

by plotting the data as $(\rho - \rho_0)/T^n$ vs. T and adjusting n and ρ_0 to produce a horizontal line. As pointed out previously,²⁸ this approach produces fitting parameters that are far less sensitive to the temperature range under consideration than when directly fitting the data to Eq. 4.

Results for CeCoIn_5 samples I and II are plotted in Fig. 6. Simultaneous measurements of $\rho_c(T)$ and $\rho_{ab}(T)$ on sample I produce fitting exponents that are essentially equivalent: $n_{ab} = 1.03 \pm 0.02$ and $n_c = 0.97 \pm 0.02$. The ab -plane resistivity begins to deviate from this linear T -dependence above 12 K, while the c -axis data show a similar deviation starting at 8 K. The ab -plane data also

deviate from the horizontal trend for $T < 4$ K, well above T_c . A similar deviation, although at a slightly lower temperature (~ 3.4 K), was observed previously²⁸ and attributed to the opening of a pseudogap. The existence of such a gap is still subject to debate²⁸ since specific heat and magnetic susceptibility measurements have yet to produce confirming evidence that it exists. As indicated in Fig. 6, c-axis measurements on sample II give practically the same result as for sample I, with a power-law exponent of $n_c = 1.00 \pm 0.02$. The data therefore reveal that the out-of-plane resistivity in CeCoIn₅ changes linearly with temperature between T_c and roughly 8 K and show no evidence for a pseudogap.

The spin fluctuation (SF) theories of non-Fermi-liquid behavior predict $n = 1$ and $n = 1.5$ for two-dimensional and three-dimensional quantum-critical (QC) systems, respectively.^{10,47,48,49,50} Recent In-NQR and Co-NMR measurements indicate that the AFM spin fluctuations in CeCoIn₅ are 3D with anisotropy such that the magnetic correlation length along the c-axis is shorter than that within the tetragonal plane.²⁶ If AFM spin fluctuations associated with a QCP are responsible for the T-linear resistivity exhibited by CeCoIn₅, then correlation-length anisotropy provides a simple explanation of why the temperature region of linear $\rho(T)$ dependence for in-plane transport is larger than for transport along the c-axis.

The discrepancy between the observed temperature exponent ($n = 1$) and that expected for 3D system ($n = 1.5$) can be clarified by taking into account the role of disorder in a 3D system. When the dual effects of isotropic impurity scattering and anisotropic spin-fluctuation scattering on $\rho(T)$ are calculated for a 3D system, $\rho \propto T^{1.5}$ behavior is only realized at very low temperatures on the order of $10^{-3}\Gamma$, where Γ is a characteristic SF energy scale.^{9,29,51} For HF systems Γ is comparable to the coherence temperature, T_{coh} .²⁹ CeCoIn₅ resistivity data indicate that $T_{coh} \approx 45$ K, so that the aforementioned very-low- T region ($T < 45$ mK) is not accessible due to the 2.3 K superconducting transition. In the experimentally accessible intermediate-temperature region transport exponents near 1.0 are expected for a clean system.⁹ Following Rosch, the inverse of the residual resistivity ratio can serve as an estimate of the degree of disorder, $x \approx \rho_{ab}(T \rightarrow 0)/\rho_{ab}(300K)$.²⁹ According to this criterion sample I with $x \approx 0.1$ is relatively clean and $n \sim 1$ is expected in the temperatures of the order of $\sim 0.1\Gamma$,⁹ and this is what we observed experimentally.

D. The magnetoresistance of CeCoIn₅ in the coherence regime

In this section we discuss the LMR of CeCoIn₅ for temperatures below the point where the zero-field resistivity exhibits a coherence peak ($T_{coh} \sim 45$ K). The data plotted in Fig. 2 clearly indicate that the LMR is generally negative and grows in magnitude with decreasing temperature. For $T < T_{coh}$ the zero-field re-

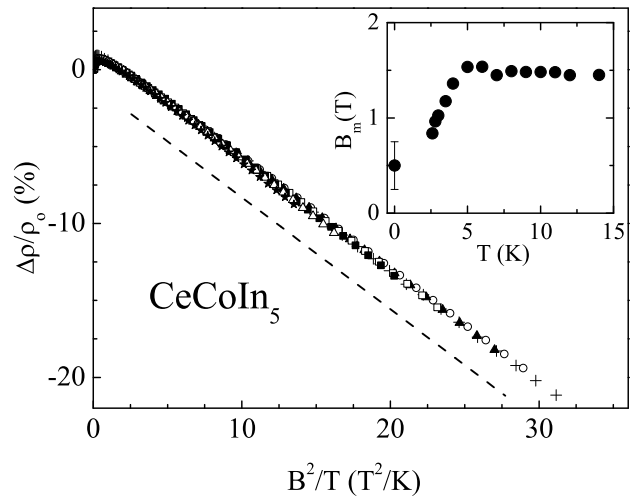


FIG. 7: LMR isotherms for CeCoIn₅ at 2.6, 2.8, 3.0, 3.5, 4, 5 and 6 K plotted as a function of B^2/T ; the dashed line is a guide to the eye. The inset shows the field of the LMR maximum B_m as a function of temperature. The B_m value at $T = 0$ comes from the zero- T extrapolations of LMR(T) data taken at different fields.

sistivity of LaCoIn₅ is minuscule compared to the resistivity of CeCoIn₅ ($\rho_{La}/\rho_{Ce} \sim 0.2\%$), and their ratio is essentially unchanged even in 9 T. As such, any conventional electronic-structure contribution to the magnetoresistance of CeCoIn₅ is negligible, and the MR of CeCoIn₅ below 20 K can be fully attributed to the presence of Ce ions and f-electrons.

We focus first on the negative contribution to the low-temperature LMR that dominates the data depicted in Fig. 2 for $B > 3$ tesla. This negative component varies quadratically with field and grows rapidly with decreasing temperature. As shown in Fig. 7 the LMR field sweeps for temperatures ranging from 6 K down to T_c can be superimposed onto a common line when the data are replotted as a function of the scaling parameter B^2/T . The c-axis resistivity shows nFL behavior ($\rho_c \propto T$) at the temperatures where the MR data scale in this way. The cause for the B^2/T LMR scaling in the nFL regime becomes clear when we parameterize the resistivity through the expression

$$\rho(B, T) = \rho_{res}(B) + \alpha(B)T. \quad (5)$$

The $\rho(B, T)$ data vary linearly with T from 1.5 K up to roughly 8 K, and the field dependence for ρ_{res} and α as extracted from linear fits to the $\rho(B, T)$ data are shown in Fig. 8. The slope is weakly field-dependent, changing by only 1.1% when the field is increased from 0 to 9 tesla. In contrast, the extrapolated residual resistivity term is quite field-dependent; beginning at $B = 0$ where ρ_{res} is essentially zero, the residual term becomes increasingly negative as B is increased, and it varies quadratically with the field strength. The $\rho(B, T)$ parametrization

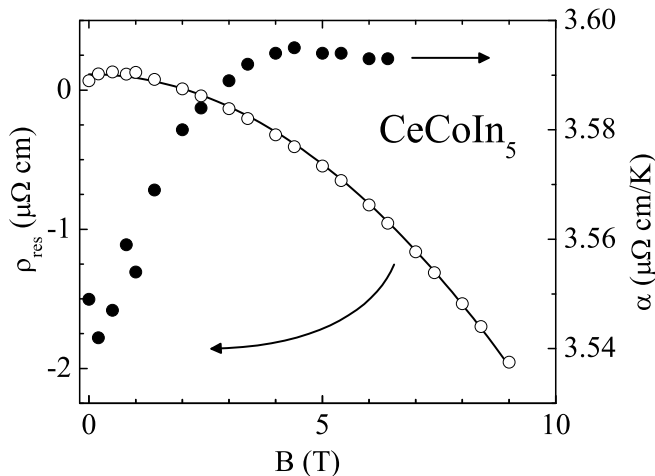


FIG. 8: Fitting parameters from constant-field CeCoIn₅ data for $1.8\text{K} \leq T \leq 8\text{K}$ plotted as a function of field. The solid line is a quadratic fit to $\rho_{res}(B)$ with a small $B = 0$ offset.

shown in Fig. 8 indicates that the applied field serves to offset the nFL resistivity downward. The B^2/T LMR scaling directly follows from (1) a field-independent slope in $\rho(T)$, (2) a negligible residual resistivity at $B = 0$, and (3) $\rho_{res} \propto -B^2$ at higher fields. The increasingly negative B -dependent residual resistivity evident from 1.5 K to 8 K is an indication that the resistivity must become a stronger function of T ($\rho \propto T^n$ with $n > 1$) at lower temperatures. Hence, the negative $\rho_{res}(B)$ term in the nFL state simply reflects the fact that the magnetic field pushes the system into a FL state at much lower temperatures. This point will be discussed further in Sec. IV E.

We turn now to the low-field range where a *positive* LMR is observed and the aforementioned B^2/T scaling no longer holds. As shown in the inset to Fig. 2 this small positive LMR appears beginning at roughly 16 K with a magnitude that increases with decreasing T , reaching a maximum value of $\sim 1\%$ near the onset of superconductivity. A low-field positive magnetoresistance is a common attribute of Kondo-lattice systems in or close to their Fermi-liquid ground-state. This behavior is exhibited, for example, by CeRu₂Si₂ (Ref. 52), CeAl₃ (Ref. 53,54), YbNi₂B₂C (Ref. 55), and CeRhIn₅ (Ref. 34). In a Kondo-lattice Fermi-liquid the MR maximum results from the competition between a T -independent residual resistivity contribution that increases in a magnetic field, and a temperature-dependent term that decreases in a magnetic field and grows quadratically with temperature.^{56,57} However, for the aforementioned Kondo-lattice case the location, B_m , of the MR maximum moves toward lower fields with increasing T , as illustrated in Fig. 3 of Ref. 53. This occurs because the negative MR component stemming from charge fluctuations grows with increasing temperature. In CeCoIn₅ the opposite trend is observed up to 6 K – the maxima shift toward *higher* fields with higher T ,

as can be seen in the inset to Fig. 2. The positions of these maxima, B_m , obtained from polynomial fits to the low-field LMR data, are shown in the inset to Fig. 7. The difference between the low-field MR in a coherent Kondo system and that of CeCoIn₅ resides in the fact that the extrapolated residual resistivity term in CeCoIn₅ produces a negative MR while a small positive MR results from the slight increase in the slope of $\rho(T)$ shown in Fig. 8. This positive component grows relative to the negative residual term with increasing temperature, resulting in B_m moving to higher fields as the temperature is increased. The field-dependent evolution of the MR in CeCoIn₅ is quite different from that of a Kondo system that does not show nFL behavior in the low- T resistivity. As such the low-field positive LMR in CeCoIn₅ is consistent with field quenching of the AFM spin fluctuations responsible for the nFL behavior.

At roughly 6 K a significant change in the LMR behavior takes place; B_m becomes T -independent above 6 K and the data no longer follow the B^2/T scaling relationship. Attempts to find any simple MR scaling in the range 7 K–20 K were unsuccessful. To clarify the possible origin of this LMR behavior we carried out Hall effect measurements on sample II below 20 K with $I \parallel c$ and the Hall voltage V_{xy} measured in the ab-plane. Two characteristic features are present in the data: first, V_{xy} varies nonlinearly with field and it changes sign as well. Second, constant-temperature $V_{xy}(B)$ curves shift toward lower values with increasing T up to 6 K, and then they start to move in the opposite direction – to higher values – above 6 K. With regard to the second effect, a shallow minimum in the Hall coefficient $R_H(T)$ centered at roughly the same temperature has been seen in ab-plane transport measurements when the field exceeded 0.5 T.³¹ This temperature dependence is typical for multi-band electronic structure system in which the weighted contribution from different bands changes with temperature.⁴⁰ The nonlinear field dependence of V_{xy} can be attributed to the Kondo interactions present in the system. When an external field is applied to a HF system, the Kondo resonance will broaden, split, and ultimately shifts below the Fermi energy.⁵⁸ When two bands are present, the response to an applied field can be different for the carries in these two bands. The band for which the field suppresses the Kondo effect more efficiently will carry a larger fraction of the aggregate transport current as the field is increased. It seems quite reasonable that this mechanism can explain the observed change in the sign of the constant-temperature Hall voltage with increasing field, while a subtle interplay between Kondo interactions and multiple bands with different carrier-mobility T -dependencies could be responsible for the change in the LMR field dependence for $T \geq 6$ K.

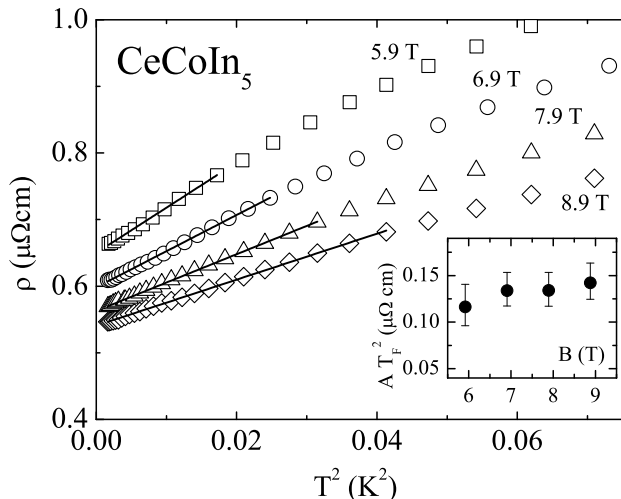


FIG. 9: The c -axis resistivity of CeCoIn_5 in the mK range plotted as a function of T^2 for fields applied parallel to the c -axis. Solid lines are linear fits from 40 mK up to $T_{FL}(B)$. The inset shows the product AT_{FL}^2 (in $\mu\Omega \text{ cm}$) plotted as a function of the field strength in tesla.

E. Restoration of Fermi-liquid behavior by magnetic field

This section is devoted to an analysis of the field-induced FL behavior evident in $\rho_c(T)$ data for large magnetic fields. Applying a magnetic field along the c -axis causes a dramatic change in the low-temperature T -dependence of ρ_c in the normal state. At 5.9 tesla the resistivity data below 130 mK can be described by the expression

$$\rho(B, T) = \rho_0(B) + A(B)T^2, \quad (6)$$

characteristic of FL behavior. The temperature range of FL behavior becomes larger with increasing field strength. The upper limit of the range where Eq. 6 is valid may be roughly identified as a characteristic temperature, T_{FL} , for the onset of Fermi-liquid behavior. T_{FL} was determined at each field using a procedure described in Ref. 59 that works as follows: a straight line was fit to the first five ρ_c vs. T^2 data points beginning at 40 mK and the resulting reduced χ^2 error was calculated. The procedure was repeated by including successive data points at higher temperature, and T_{FL} was determined as the temperature T_χ where χ^2 starts to grow rapidly. Plots of $(\rho - \rho_0)/T^2$ at different field strengths were also used to determine T_{FL} as precisely as possible. In the Landau FL theory the coefficient A in Eq. 6 is inversely proportional to the square of the characteristic temperature governing the FL behavior. The calculated product AT_{FL}^2 is depicted in the inset to Fig. 9; the error bars reflect the uncertainty in determining the position of T_χ following the procedure described above. Within these error bars AT_{FL}^2 is constant, confirming the consistency of our analysis.

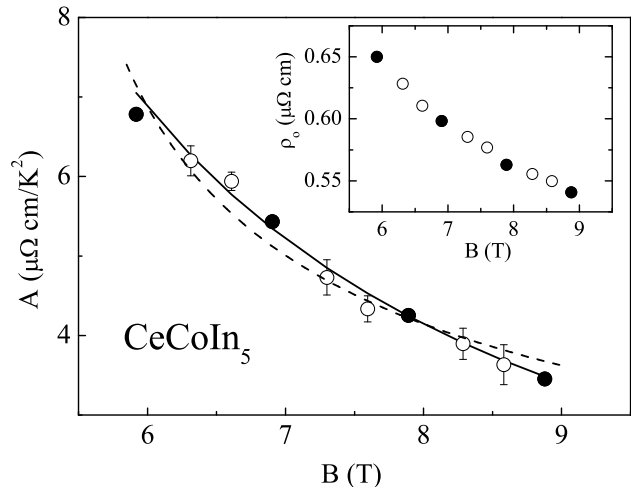


FIG. 10: The T^2 resistivity coefficient A plotted as a function of field. The solid and open symbols correspond to temperature-sweep and field-sweep data, respectively. The solid line shows the least-squares fit to Eq. 7 when setting $p = 1.37$; the fit gives $B_{cr} = 1.5 \pm 0.2$ T. The dashed line shows the fit when setting $B_{cr} = B_{c2}$. Field-dependent ρ_0 values are shown in the inset.

We now use the field dependence of the coefficient A to determine the location of the QCP in CeCoIn_5 in relation to the c -axis upper critical field $B_{c2} = 4.95$ tesla.^{60,61} Values of A at different fields, taken both from fits to $\rho_c(T)$ data taken at various fields and from $\rho_c(B)$ data taken at various temperatures, are shown in Fig. 10. The data indicate that A is a decreasing function of field, an entirely expected result given that this coefficient is a measure of the strength of quasi-particle-quasi-particle interactions, and, as such, is proportional to the effective mass. We fit the data to a formula that models the diverging behavior of A ,

$$A(B) = \frac{A_0}{(B - B_{cr})^p}, \quad (7)$$

where B_{cr} is the critical field where A diverges, p is the critical exponent ($p > 0$), and A_0 is a constant. The dynamic range over which $A(B)$ can be measured is limited because the superconducting ground-state masks the FL transport behavior for fields less than roughly 6 tesla. For this reason determining B_{cr} and p unambiguously requires care when analyzing the data. A plot of $1/A$ vs. B shows upward curvature, indicating that $p > 1$. An upper limit on B_{cr} can be obtained if we fix p to 1 and perform a non-linear least-squares fit to the data; this approach gives $B_{cr} = (3 \pm 0.2)$ tesla, a value that is clearly less than B_{c2} . If we use $p = 1.37$ as determined from ab-plane transport³⁰ and specific-heat measurements,²⁵ the best-fit to the data (the solid line in Fig. 10) gives $B_{cr} = (1.5 \pm 0.2)$ tesla, putting the QCP even farther into the superconducting state. If, alternatively, we force the critical field to coincide with B_{c2} , the resulting best-fit

critical exponent ($p = 0.5$) provides a very poor description of the data. This fit, depicted in Fig. 10 as a dashed line, has a χ^2 error 10 times greater than that for the fit that gives $B_{cr} = 1.5$ tesla. Clearly, the c-axis transport data are inconsistent with B_{cr} being close to B_{c2} , but instead places the QCP well inside the superconducting phase. In a very qualitative sense the negative values of $\rho_{res}(B)$ obtained for fields greater than roughly 2 tesla (see Fig. 8) are also consistent with this conclusion. Interestingly, a linear fit to a plot of ρ_0/A vs. B gives a zero-intercept at $B_{cr} = (1.7 \pm 0.4)$ T, i.e. at the same field (within the error bars) as B_{cr} determined from the fit with $p = 1.37$. As shown in the inset to Fig. 3 the magnetoresistance is affected by superconducting fluctuations for fields below 5.9 T. This precludes enhancing the dynamic range of the data by determining A at lower fields. Despite the limited field range used in the analysis, c-axis transport data clearly suggest that the critical point resides well inside the superconducting phase.

This conclusion appears to be at odds with ab-plane transport and specific heat measurements^{25,30,62,63} which show rather clearly that the critical point coincides with B_{c2} . Those measurements indicate that, despite a factor of 2.4 difference in B_{c2} for $B \perp c$ and $B \parallel c$, B_{cr} tracks B_{c2} for either field direction.^{25,30,63} Even more compelling is the fact that B_{cr} still coincides with B_{c2} when the critical field is reduced by 50% through Sn doping.⁶² These results indicate that it is more than just a coincidence that the critical field occurs at B_{c2} . Why, then, do c-axis magnetotransport data place B_{cr} far below B_{c2} ? The complexities intrinsic to the electronic structure of CeCoIn₅ may be responsible. Band structure calculations and de Haas-van Alphen measurements indicate the Fermi surface of CeCoIn₅ is composed of 3D hole pockets and c-axis oriented 2D electron-like sheets.^{18,41} While ab-plane transport involves carriers on both pieces of the Fermi surface, c-axis transport will be carried predominately by the 3D pockets. Given the large anisotropy in B_{cr} and B_{c2} , it is not unreasonable to conclude that critical fluctuations are more prevalent on the 2d sheets. If true, c-axis transport would not be heavily influenced by fluctuations associated with the QCP, but would instead reflect a more complicated mix of

field-dependent transport effects. These magnetotransport complications could alter our critical point analysis sufficiently to mask the true location of B_{cr} .

V. CONCLUSIONS

The c-axis transport of CeCoIn₅ is dominated by single-impurity Kondo scattering at high temperatures while AFM critical fluctuations associated with a nearby QCP control the transport at low temperatures. Between 50 and 100 K the longitudinal magnetoresistance of this Kondo lattice compound is consistent with a single-impurity Kondo energy scale of roughly 2 K. Below 10 K the T -linear nFL behavior of both ρ_{ab} and ρ_c are consistent with anisotropic 3D AFM spin fluctuations in a relatively clean system. As in previous ab-plane studies,³⁰ applying a magnetic field along the c-axis restores FL behavior at low temperatures. In sharp contrast to those ab-plane magnetotransport measurements, the field dependence of ρ_c in the field-induced FL regime suggests that the QCP in CeCoIn₅ resides well inside the superconducting phase; this result is at odds with a number of ab-plane transport and thermodynamic measurements which place the critical point at B_{c2} . The magnetic fluctuations associated with the QCP influence the transport properties at least up to 16 K. The influence that these fluctuations have on the electronic transport are reduced by increasing the temperature or applying a magnetic field to the system. For large fields the LMR becomes negative as the system is pushed away from the QCP. Changes in the LMR field dependence above 6 K suggest that the complex multiband electronic structure strongly influences the B -dependent electronic transport in CeCoIn₅.

Acknowledgments

We thank Z. Fisk and J. Lawrence for useful discussions. This work was performed under auspices of the U.S. Department of Energy.

* Present address: Department of Physics and Astronomy, Louisiana State University, Baton Rouge, LA 70803.

¹ G. R. Stewart, Rev. Mod. Phys. **73**, 797 (2001).

² M. B. Maple, M. C. deAndrade, J. Herrmann, Y. Dalichaouch, D. A. Gajewski, C. L. Seaman, R. Chau, R. Movshovich, M. C. Aronson, and R. Osborn, J. Low Temp. Phys. **99**, 223 (1995).

³ M. Gurvitch and A. T. Fiory, Phys. Rev. Lett. **59**, 1337 (1987).

⁴ H. L. Stormer, A. F. J. Levi, K. W. Baldwin, M. Anzlowar, and G. S. Boebinger, Phys. Rev. B **38**, 2472 (1988).

⁵ P. Schlottmann, J. Appl. Phys. **89**, 7183 (2001).

⁶ O. O. Bernal, D. E. MacLaughlin, H. G. Lukefahr, and B. Andraka, Phys. Rev. Lett. **75**, 2023 (1995).

⁷ E. Miranda, V. Dobrosavljević, and G. Kotliar, J. Phys.: Condens. Matter **8**, 9871 (1996).

⁸ A. H. CastroNeto, G. Castilla, and B. A. Jones, Phys. Rev. Lett. **81**, 3531 (1998).

⁹ A. Rosch, Phys. Rev. Lett. **82**, 4280 (1999).

¹⁰ A. J. Millis, Phys. Rev. B **48**, 7183 (1993).

¹¹ M. J. Graf, R. J. Keizer, A. de Visser, and S. T. Hannahs, Physica B **284-288**, 1281 (2000).

¹² S. Kambe, S. Raymond, H. Suderow, J. M. Donough, B. F. k, L. P. Regnault, R. Calemczuk, and J. Flouquet, Physica

- B **223&224**, 135 (1996).
- ¹³ O. Stockert, H. v. Lohneysen, A. Rosch, N. Pyka, and M. Loewenhaupt, *Phys. Rev. Lett.* **80**, 5627 (1998).
 - ¹⁴ V. V. Krishnamurthy, K. Nagamine, I. Watanabe, K. Nishiyama, S. Ohira, M. Ishikawa, D. H. Eom, and T. Ishikawa, *Physica B* **289-290**, 47 (2000).
 - ¹⁵ S. L. Sondhi, S. M. Girvin, J. P. Carini, and D. Shahar, *Rev. Mod. Phys.* **69**, 315 (1997).
 - ¹⁶ A. M. Tselik and M. Reizer, *Phys. Rev. B* **48**, R9887 (1993).
 - ¹⁷ C. Petrovic, P. G. Pagliuso, M. F. Hundley, R. Movshovich, J. L. Sarrao, J. D. Thompson, Z. Fisk, and P. Monthoux, *J. Phys.: Condens. Matter* **13**, L337 (2001).
 - ¹⁸ R. Settai, H. Shishido, S. Ikeda, Y. Murakawa, M. Nakashima, D. Aoki, Y. Haga, H. Harima, Y. Onuki, and P. Schlottmann, *J. Phys.: Condensed Matter* **13**, L627 (2001).
 - ¹⁹ D. Hall, E. C. Palm, T. P. Murphy, S. W. Tozer, C. Petrovic, E. Miller-Ricci, L. Peabody, C. Q. H. Li, U. Alver, R. G. Goodrich, et al., *Phys. Rev. B* **64**, 064506 (2001).
 - ²⁰ R. Movshovich, M. Jaime, J. D. Thompson, C. Petrovic, Z. Fisk, P. G. Pagliuso, and J. L. Sarrao, *Phys. Rev. Lett.* **86**, 5152 (2001).
 - ²¹ Y. Kohori, Y. Yamato, Y. Iwamoto, T. Kohara, E. D. Bauer, M. B. Maple, and J. L. Sarrao, *Phys. Rev. B* **64**, 134526 (2001).
 - ²² K. Izawa, H. Yamaguchi, Y. Matsuda, H. Shishido, R. Settai, and Y. Onuki, *Phys. Rev. Lett.* **87**, 057002 (pages 4) (2001).
 - ²³ H. Aoki, T. Sakakibara, H. Shishido, R. Settai, Y. Onuki, P. Miranovic, and K. Machida, *J. Phys.: Condens. Matter* **16**, L13 (2004).
 - ²⁴ S. Nakatsuji, S. Yeo, L. Balicas, Z. Fisk, P. Schlottmann, P. G. Pagliuso, N. O. Moreno, J. L. Sarrao, and J. D. Thompson, *Phys. Rev. Lett.* **89**, 106402 (2002).
 - ²⁵ A. Bianchi, R. Movshovich, I. Vekhter, P. G. Pagliuso, and J. L. Sarrao, *Phys. Rev. Lett.* **91**, 257001 (2003).
 - ²⁶ Y. Kawasaki, S. Kawasaki, M. Yashima, T. Mitro, G. Zheng, Y. Kitaoka, H. Shishido, R. Settai, Y. Haga, and Y. Onuki, *J. Phys. Soc. Jap.* **72**, 2308 (2003).
 - ²⁷ J. S. Kim, J. Alwood, G. R. Stewart, J. L. Sarrao, and J. D. Thompson, *Physical Review B (Condensed Matter and Materials Physics)* **64**, 134524 (2001).
 - ²⁸ V. A. Sidorov, M. Nicklas, P. G. Pagliuso, J. L. Sarrao, Y. Bang, A. V. Balatsky, and J. D. Thompson, *Phys. Rev. Lett.* **89**, 157004 (2002).
 - ²⁹ A. Rosch, *Phys. Rev. B* **62**, 4945 (2000).
 - ³⁰ J. Paglione, M. A. Tanatar, D. G. Hawthorn, E. Boaknin, R. W. Hill, F. Ronning, M. Sutherland, L. Taillefer, C. Petrovic, and P. C. Canfield, *Phys. Rev. Lett.* **91**, 246405 (2003).
 - ³¹ M. F. Hundley, A. Malinowski, P. G. Pagliuso, J. L. Sarrao, and J. D. Thompson, *Phys. Rev. B* **70**, 035113 (2004).
 - ³² L. J. van der Pauw, *Philips Res. Rep.* **13**, 1 (1958).
 - ³³ W. L. V. Price, *Solid-State Electron.* **16**, 753 (1973).
 - ³⁴ A. D. Christianson, A. H. Lacerda, M. F. Hundley, P. G. Pagliuso, and J. L. Sarrao, *Phys. Rev. B* **66**, 054410 (2002).
 - ³⁵ See, e.g., N. Grewe and F. Steglich, in *Handbook on the Physics and Chemistry of Rare Earth*, edited by K.A. Gschneider, Jr. and L. Eyring (Elsevier, Amsterdam, 1991), vol. 14, p. 343.
 - ³⁶ For one of the recent review, see: A. S. Edelstein, *Journ. Mag. Mag. Mat.* **256**, 430 (2003).
 - ³⁷ See, e.g., J. M. Ziman, *Electrons and Phonons*, (Oxford University Press, Oxford, 1960), p. 491.
 - ³⁸ R. G. Chambers, *Proc. Roy. Soc (London)* **238**, 344 (1956).
 - ³⁹ A. B. Pippard, *Magnetoresistance in Metals* (Cambridge University Press, Cambridge, 1989), p. 23.
 - ⁴⁰ C. M. Hurd, *The Hall effect in metals and alloys* (Plenum Press, New York, 1972).
 - ⁴¹ H. Shisido, R. Settai, D. Aoki, S. Ikeda, H. Nakawaki, N. Nakamura, T. Iizuka, Y. Inada, K. Sugiyama, T. Takeuchi, et al., *J. Phys. Soc. Jap.* **71**, 162 (2002).
 - ⁴² Y. Haga, Y. Inada, H. Harima, K. Oikawa, M. Murakawa, H. Nakawaki, Y. Tokiwa, D. Aoki, H. Shishido, S. Ikeda, et al., *Phys. Rev. B* **63**, 060503(R) (2001), dHvA on CeIrIn5.
 - ⁴³ C. M. Hurd, *The Hall Effect in Metals and Alloys* (Plenum Press, New York, 1972), chap. 2.
 - ⁴⁴ A. A. Abrikosov, *Introduction to the Theory of Normal Metals* (Academic Press, New York and London, 1972), vol. 12 of *Solid State Physics*, chap. 6, pp. 121–122.
 - ⁴⁵ P. Schlottmann, *Phys. Rep.* **181**, 1 (1989).
 - ⁴⁶ B. Coqblin and J. R. Schrieffer, *Phys. Rev.* **185**, 847 (1969).
 - ⁴⁷ J. A. Hertz, *Phys. Rev. B* **14**, 1165 (1976).
 - ⁴⁸ T. Moriya and T. Takimoto, *J. Phys. Soc. Jpn.* **64**, 960 (1995).
 - ⁴⁹ G. G. Lonzarich, *The Electron* (edited by M. Springford, Cambridge University Press, Cambridge/New York, 1997), chap. 6.
 - ⁵⁰ S. Sachdev, *Quantum Phase Transitions* (Cambridge University Press, Cambridge, England, 1999).
 - ⁵¹ A. Rosch, *J. Mag. Mag. Mat.* **226-230**, 11 (2001).
 - ⁵² J. Flouquet, P. Haen, F. Lapiere, D. Jaccard, and G. Remenyi, *J. Magn. Mag. Mat.* **54-57**, 322 (1986).
 - ⁵³ J. G. M. Roesler and P. M. Tedrow, *Physica B* **165&166**, 419 (1990).
 - ⁵⁴ G. M. Roesler and P. M. Tedrow, *Phys. Rev. B* **45**, 12893 (1992).
 - ⁵⁵ A. Yatskar, C. H. Mielke, P. C. Canfield, A. H. Lacerda, and W. P. Beyermann, *Phys. Rev. B* **60**, 8012 (1999).
 - ⁵⁶ F. J. Ohkawa, *Phys. Rev. Lett.* **64**, 2300 (1990).
 - ⁵⁷ C. Chen, Z.-Z. Li, and W. Xu, *J. Phys.: Condens. Matter* **5**, 95 (1993).
 - ⁵⁸ K. Satoh, T. Fujita, Y. Maeno, Y. Onuki, T. Komatsubara, T. Ohtsuka, and P. Schlottmann, *Solid State Commun* **56**, 327 (1985).
 - ⁵⁹ R. P. Dickey, M. C. de Andrade, J. Herrmann, M. B. Maple, F. G. Aliev, and R. Villar, *Phys. Rev. B* **56**, 11169 (1997).
 - ⁶⁰ T. P. Murphy, D. Hall, E. C. Palm, S. W. Tozer, C. Petrovic, Z. Fisk, R. G. Goodrich, P. G. Pagliuso, J. L. Sarrao, and J. D. Thompson, *Phys. Rev. B* **65**, 100514(R) (2002).
 - ⁶¹ S. Ikeda, H. Shishido, M. Nakashima, R. Settai, D. Aoki, H. Yoshinori, H. Hisatomo, A. Yuji, N. Takahiro, S. Hideyuki, et al., *J. Phys. Soc. Japan* **70**, 2248 (2001).
 - ⁶² E. D. Bauer, C. Capan, F. Ronning, R. Movshovich, J. D. Thompson, and J. L. Sarrao, unpublished.
 - ⁶³ F. Ronning, C. Capan, A. Bianchi, R. Movshovich, A. Lacerda, M. F. Hundley, J. D. Thompson, P. G. Pagliuso, and J. L. Sarrao, unpublished.